

# Self-assembly of complex structures in colloid-polymer mixtures

Erdal C. Oğuz,<sup>1,2,\*</sup> Aleksandar Mijailović,<sup>1,3</sup> and Michael Schmiedeberg<sup>3</sup>

<sup>1</sup>*Institut für Theoretische Physik II, Heinrich-Heine Universität,  
Universitätsstr. 1, 40225 Düsseldorf, Germany*

<sup>2</sup>*School of Mechanical Engineering and The Sackler Center for Computational  
Molecular and Materials Science, Tel Aviv University, Tel Aviv 6997801, Israel*

<sup>3</sup>*Institut für Theoretische Physik 1, Friedrich-Alexander-Universität  
Erlangen-Nürnberg, Staudtstr. 7, 91058 Erlangen, Germany*

(Dated: February 19, 2022)

If particles interact according to isotropic pair potentials that favor multiple length scales, in principle a large variety of different complex structures can be achieved by self-assembly. We present, motivate, and discuss a conjecture for the occurrence of non-trivial (i.e., non-triangular) orderings based on newly-introduced enthalpy-like pair potentials, the capability of which we demonstrate for the specific example of colloid-polymer mixtures. Upon examining the phase behavior of two-dimensional colloid-polymer mixtures, which can also be realized in experiments, we observe that non-trivial structures only occur in the vicinity of selected densities where triangular ordering is suppressed by the pair potential. Close to these densities, a large number of different phases self-assemble that correspond to tilings containing triangular, rhombic, square, hexagonal, and pentagonal tiles, and including some of the Archimedean tilings. We obtain the ground-state energies by minimizing the corresponding lattice sums with respect to particle positions in a unit cell as well as cell geometry and verify the occurrence of selected phases at finite temperatures by using Brownian Dynamics simulations. All reported phases should be accessible in experiments and, in addition, our work provides a manual on how to find the regions of non-trivial phases in parameter space for complex pair interactions in general.

## I. INTRODUCTION

Self-assembly is the process by which the system constituents form large organized functional units via their mutual interactions without any external influence. Since the pioneering work by Whitesides et al. [1] on molecular systems, self-assembly has been studied in great detail in a wide range of length scales ranging from atomic to macroscopic systems and throughout various scientific disciplines, including physics, chemistry, materials science, and biology [2–14].

In monodisperse systems that do not possess more than one characteristic length scale self-assembly usually occurs in the same way as for hard disks or spheres, i.e., the particles form a triangular phase in two or a fcc-crystal in three dimensions and at appropriate conditions. Beyond such simple systems, a plethora of self-assembled complex structures can be achieved in mixtures of different particle types such as in metallic alloys [15] or in binary colloidal suspensions [16–18]. Two further scenarios pave the way for high structural complexity in one-component systems by requiring *i*) an interaction or shape anisotropy and *ii*) a deliberate choice of an isotropic pair interaction with multiple length scales that affect the structure formation. Prototypical examples of the former are hard convex polyhedra packings [19] and patchy colloids [20–22], whereas concerning the latter inverse statistical-mechanical approaches have been undertaken to investigate the self-assembly of

non-triangular ground-state structures with engineered pair interaction potentials [23–26]. More recently it has even been shown that complex ground-state structures can be stabilized by repulsive and convex pair interaction potentials which rule out the necessity for single- or multiple wells in this potential [27–32]. Unfortunately, the interactions obtained by the aforementioned inverse construction methods are most often artificial and in the consequence hard to realize in experiments.

A system that is well-studied in theory and simulation and in addition can be realized and investigated experimentally is a charge-stabilized colloid-polymer mixture which intrinsically involves multiple length scales as the colloids effectively attract each other close to contact due to depletion interactions while being repulsive on larger length scales because of screened electrostatic repulsions. Experimental and theoretical studies have been performed to understand the nature of colloid-polymer mixtures [33–44] some of which exhibit glassy states [36, 37], gels [38–42], and cluster formation [41, 43, 44]. The phase behavior concerning the gas, liquid, and trivial solid phase has been investigated in [45–55]. Moreover, the influence of many-body interactions on the phase behavior of such mixtures [56, 57] as well as confinement effects [58–61] have been analyzed recently. However, to the best of our knowledge, detailed structural analysis of the crystal phase were not in the focus of previous studies, nor any non-trivial complex ordering have been reported with the exception of local ground-state clusters [41, 44].

In this article, we determine the ground states that occur in a colloid-polymer mixture in two dimensions. The ground-state orderings are calculated by minimiz-

\* erdaloguz@mail.tau.ac.il

ing the energy for structures with one to six particles per unit cell. Aside from the trivial triangular phase, we observe square, rhombic, triangular, honeycomb, Kagome, and Archimedean tilings [62–65] as well as further orderings that correspond to tilings with hexagons and even pentagons.

In order to understand why non-trivial structures in monodisperse systems with isotropic interactions can occur in general, we introduce an enthalpy-like pair potential and conjecture that it can be used in order to identify the parameters such that triangular structures are suppressed. Our approach explains why and how even monotonic pair potentials can be used in order to self-assemble complex phases.

## II. SYSTEM AND METHODS

### A. Colloid-polymer mixtures

When immersed in a solvent of relatively small-sized non-adsorbing polymer coils, the larger colloidal particles sense a short-ranged *depletion* attraction at sufficiently high polymer concentrations. This attractive force arises due to an unbalanced osmotic pressure stemming from the depletion zone in the region between the colloids.

The effective pair interaction potential between point-like colloids in the presence of the polymers is given by a screened Coulomb repulsion corresponding to a Yukawa-like interaction, and on short lengths by depletion attraction where we employ the AO-model [66, 67]. Therefore, the pair interaction potential is

$$v(r_{ij}) = \begin{cases} V_0 \frac{\exp(-\kappa r_{ij})}{\kappa r_{ij}} - W_0 \left[ 1 - \frac{3r_{ij}}{2d} + \frac{r_{ij}^3}{2d^3} \right] & \text{if } r_{ij} \leq d, \\ V_0 \frac{\exp(-\kappa r_{ij})}{\kappa r_{ij}} & \text{if } r_{ij} > d, \end{cases} \quad (1)$$

where  $r_{ij}$  is the separation distance between colloids  $i$  and  $j$ ,  $\kappa$  denotes the inverse screening length, and  $d$  the depletion length dictating the range of the attractive interaction and corresponding to the typical diameter of the polymers. The energy amplitude of the pure electrostatic Yukawa interaction is given by  $V_0$ , whereas the strength of the depletion potential is set by  $W_0$ . The crystalline phase diagrams can therefore be determined in three-dimensional space spanned by the reduced energy amplitude  $V_0/W_0$ , the reduced density  $\sqrt{\rho}d$ , and the reduced depletion length  $\kappa d$  corresponding to the ratio of depletion length divided by screening length.

We primarily explore the ground state of our model colloid-polymer mixtures by determining the corresponding phase diagrams in the  $(\sqrt{\rho}d, \kappa d)$ -plane at fixed  $V_0/W_0$ . At zero-temperature, the optimal structures with  $N$  particles are those that minimize the total in-

ternal energy

$$U = \frac{1}{2} \sum_{\substack{i,j \\ i \neq j}}^N v(r_{ij}) \quad (2)$$

at a given reduced density, depletion length, and energy amplitude. We use a direct lattice summation technique to determine  $U$ , and thus to predict the corresponding ground-state structures. In order to examine the stability of resulting structures at finite temperatures, we extend our studies to  $T > 0$  by means of Brownian Dynamics computer simulations. In the following, we provide details for both the lattice summation and the finite-temperature simulations used in this work.

### B. Lattice-sum calculations

At each given density  $\sqrt{\rho}d$ , depletion length  $\kappa d$ , and energy amplitude  $V_0/W_0$ , we have performed lattice sum minimizations for a set of candidates of crystalline lattices. As possible candidates, we consider two-dimensional crystals with a periodicity in both the spatial directions  $x$  and  $y$  whose primitive cell is a parallelogram containing  $n$  particles. This parallelogram is spanned by the two lattice vectors  $\mathbf{a} = a(1, 0)$  and  $\mathbf{b} = a\gamma(\cos \theta, \sin \theta)$ , where  $\gamma$  denotes the aspect ratio ( $\gamma = |\mathbf{b}|/|\mathbf{a}| = b/a$ ), and  $\theta$  is the angle between  $\mathbf{a}$  and  $\mathbf{b}$ . We consider candidates with primitive cells comprising up to 6 particles, i.e.,  $n = 1, \dots, 6$ , with no further restrictions.

At prescribed parameters, the total potential energy per particle  $u = U/N$  (cf. Eq. 2) is minimized with respect to the particle coordinates of the basis, and the cell geometry. The latter includes a minimization process of  $\gamma$  and  $\theta$ . To be specific, we implement the Nelder-Mead method (also known as downhill simplex method or amoeba method) to find the minimum of the energy functions without calculating their derivatives [68]. As this technique is a heuristic approach, and thus it may not always converge to the global minimum, we use at least 200 and at most 1000 different start configurations depending on the complexity of those functions.

### C. Enthalpy-like pair potential

We introduce a new pair potential that corresponds to an enthalpy-like quantity  $h(r_{ij})$ . This enthalpy-like pair potential should be given such that the total enthalpy is

$$H = \frac{1}{2} \sum_{i,j,i \neq j}^N h(r_{ij}) = U + pA, \quad (3)$$

where  $p$  is the macroscopic pressure and  $A$  the total area of the system (in three dimensions the volume has

to be used instead). The enthalpy-like pair potential therefore can be introduced as

$$h(r) = v(r) + 2\frac{p}{N}a(r), \quad (4)$$

where  $a(r)$  is an effective surface area between any two particles at a relative distance  $r$ , which we refer to as the *pair area* in the following. The pair area  $a(r)$  has to follow from a subdivision of the total area  $A$  as in

$$NA = \sum_{\substack{i,j \\ i \neq j}}^N a(r_{ij}). \quad (5)$$

Note that  $a(r_{ij})$  shall be given such that for a fixed particle  $i$ , a summation over  $j$  leads to  $A$ . Then, a summation over all  $i$  and  $j$  with  $i \neq j$  yields a total area of  $NA$ .

In order to get an idea what the enthalpy-like pair potential can look like, we consider a particle  $i$  and its  $k$  neighbor shells. The remaining  $N - 1$  particles are distributed over these  $k$  shells. We denote the  $k$ th shell of  $i$ , to which the particle  $j$  belongs, by the index  $k_{ij}$ , its thickness by  $\delta_{k_{ij}}$ , its relative position to the particle  $i$  by  $r_{k_{ij}}$ , and the corresponding coordination number by  $Z_{k_{ij}}$ . Consequently, the pair area  $a(r_{ij})$  can be written as the area of the  $k$ th shell of particle  $i$  to which the particle  $j$  belongs as

$$a(r_{ij}) \simeq \frac{2\pi}{Z_{k_{ij}}} \delta_{k_{ij}} r_{k_{ij}}, \quad (6)$$

where  $1/Z_{k_{ij}}$  compensates the counting of multiple particles in the same shell so that each shell contributes only once to the sum in Eq. 5. While the coordination number can be easily obtained from the theta series of lattices, the most common ones of which being tabulated in [69, 70], the choice of thickness  $\delta_k$  is rather not unique as the space can be subdivided differently into circular non-overlapping rings under the constraint that each of which contain solely one neighbor shell. In general, the pair area can be written as  $a(r) = f(r)r$ , where  $f(r)$  denotes the thickness  $\delta$  of a shell at a distance  $r$ . On average,  $f(r)$  is a decaying function with distance as the neighbor shells become closer to each other for large  $k$ . A canonical choice for the thickness would be  $\delta_k = (r_{k+1} - r_{k-1})/2$ , where the shell positions  $r_k$  could be gained from the radial distribution function of the structure. However, within the range of the first few neighbor shells,  $\delta_k$  can be chosen to be a constant. The value of  $Z_k$  behaves similarly in the same range. For example, in case of the triangular lattice, the first three shells possess  $Z_k = 6$  particles ( $k = 1, 2, 3$ ). Usually, only the closer neighbors will play the predominant role for the stability. If this is the case, we finally find the following approximate functional form for the pair area  $a(r)$  for distances corresponding to a few inner neighbor shells:

$$a(r) \approx C(\rho, Z, \tilde{\delta})\kappa r, \quad (7)$$

where the density-dependent prefactor  $C(\rho, Z, \tilde{\delta})$  incorporates a constant coordination number  $Z$  and a constant reduced thickness  $\tilde{\delta} = \delta/a_1$  for the first few shells with  $a_1$  being the nearest-neighbor distance, but approximately no dependence on  $r$ .

## D. Brownian Dynamics computer simulations

To study the validity of our theoretical ground-state predictions at finite but relatively low temperatures, we employ Brownian Dynamics computer simulations in the  $NVT$ -ensemble by solving the Langevin equation for an overdamped system. The position  $\mathbf{r}_i$  of particle  $i$  undergoing Brownian motion after a time step  $\delta t$  is

$$\mathbf{r}_i(t + \delta t) = \mathbf{r}_i(t) + \frac{D}{k_B T} \mathbf{F}_i(t) \delta t + \delta \mathbf{W}_i, \quad (8)$$

where  $D$  denotes the free diffusion coefficient,  $k_B T$  the thermal energy, and  $\mathbf{F}_i$  is the total conservative force acting on particle  $i$  and stemming from the pair interaction  $v$  in Eq. 1. The random displacement  $\delta \mathbf{W}_i$  is sampled from a Gaussian distribution with zero mean and variance  $2D\delta t$  (for each Cartesian component) fixed by the fluctuation-dissipation relation. The time step is chosen as  $\delta t = 10^{-5}\tau$  where  $\tau = 1/(\kappa^2 D_0)$  is used as the unit of the time. We run simulations for up to  $10^5\tau$ , starting from a random distribution, a triangular or a square lattice of  $N = 2000$  particles in a rectangular simulation box under periodic boundary conditions. All three runs yield the same final configurations at predetermined density and depletion length, suggesting the thermodynamical stability of our results rather than possible metastable configurations.

It is noteworthy that more sophisticated simulation algorithms making use of non-rectangular simulation boxes [71] might yield stable phases which we are not able to capture here in our simulations. This being said, however, we do not expect a radical change in the morphology of the phase diagram; In soft systems, the coexistence between two main phases will most likely suppress the occurrence of subtle phases with free-energies relatively close to each other and to the aforementioned main phases. Moreover, we want to emphasize that our main goal lies in determining the ground-state of colloid-polymer mixtures, where we consider non-rectangular boxes, and comparing the results to the predictions of our enthalpy-based theory, where simulations shall only serve as an additional supportive data to strengthen our findings.

In the following, we present the results from both the zero-temperature lattice-sum minimizations and the finite-temperature simulations.

## III. RESULTS

Before delving into the phase diagram for the given example of colloid-polymer mixtures in detail, i.e., de-

termining each single phase structure at prescribed density and depletion length, we first explore the conditions that lead to the formation of non-trivial structures.

### A. Enthalpy-like pair potential and occurrence of non-triangular phases

As shown in Fig. 1, for colloid-polymer mixtures, the non-triangular crystalline phases only occur in special parameter regions. These regions are marked in Fig. 1 in yellow for ground states as determined by minimizing the interaction energy. The red area indicates the phase space within which complex non-triangular structures are expected to become stable according to our enthalpy-based theory. On the one hand, the lattice-sum minimization process yields precise results (within the numerical accuracy), and as such, the corresponding ground-state phase diagram is accurate. On the other hand, our theory delivers a good estimate for the occurrence of complex non-triangular phases if their stability is dominated by the closest neighbors. Among these non-triangular phases are the complex structures with two length scales that are sufficiently distinct from the triangular length scale such as in case of the honeycomb lattice.

The differences between zero and non-zero temperature are discussed in the next subsection, and the non-triangular structures are analyzed in detail in Sec. III C. In the following, we first explore the stability of non-triangular phases in detail, and we describe our novel theoretical approach for the occurrence of complex non-triangular orderings.

The triangular lattice can be stabilized by various types of two-body interactions, among which are those that are purely repulsive and that involve one simple length scale. For example, a screened Coulomb potential (corresponding to a Yukawa interaction), which is widely used to model charge-stabilized colloidal suspensions, leads to triangular ordering. As opposed to such interactions, the presence of multiple length scales in the pair interaction potential might yield two-dimensional crystals other than the triangular lattice [26]. For example, the interparticle forces in the colloid-polymer mixture are dictated by two different length scales that define the ranges of the attraction and the repulsion.

In order to understand the nature of non-triangular stability modes, we first consider the explicit form of the pair interaction in Eq. (1), characteristic examples of which are shown in Fig. 2 at different reduced depletion lengths  $\kappa d$  and at  $V_0/W_0 = 1$ . For large  $\kappa d = 1.8$ , a single well occurs with a clear local maximum slightly below the reduced depletion length (the positions of which are indicated by dashed lines). We find that the non-triangular structures occur at reduced densities where the depletion length  $d$  approximately corresponds to the  $k$ th next-neighbor distance  $a_k$  of the triangular lattice with  $k = 1, \dots, 5$ , cf. Fig. 1. These distances are  $a_1, a_2 = \sqrt{3}a_1, a_3 = 2a_1, a_4 = \sqrt{7}a_1$ , and

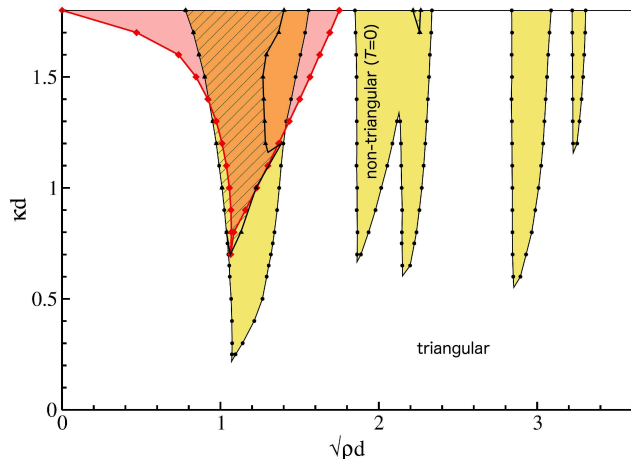


FIG. 1. Ground-state phase diagram of colloid-polymer mixtures as a function of the reduced density  $\sqrt{\rho}d$  and the reduced depletion length  $\kappa d$ . The majority of the phase space (white area) is governed by the triangular phase, whereas non-triangular phases can be stabilized around certain values of the reduced density and along the reduced depletion length. These non-triangular stability modes as determined by lattice-sum minimizations are shown by yellow regions. The actual determined phase points at the boundary are indicated by black dots. The red region indicates the theoretically predicted stability zone where complex non-triangular structures with two different length scales that are sufficiently distinct from the triangular length scale are expected to become stable. The hatched non-triangular subdomain comprises such stable complex phases as obtained by lattice-sum minimizations where the closest-neighbor distance deviates at least fifteen percent from the triangular lattice constant.

$a_5 = 3a_1$  with  $a_1 \approx 1/\sqrt{\rho}$ . In other words; the triangular lattice is suppressed at densities where its interparticle distances roughly correspond to the depletion length of the system and thus being in the close vicinity of the maximum of the potential yielding an increase in the energy of the triangular lattice. The system will therefore possess lower potential energy for structurally more complex crystals with separated length scales or for rhombic or square lattice.

Non-triangular phases are still present at low reduced depletion lengths where the pair interaction potential does not possess a local maximum, e.g., for  $\kappa d = 1.2$  as shown by the red curve in Fig. 2. Therefore, the triangular order can even be suppressed without a maximum in the pair interaction potential. Note that the presence of concavity is also not a necessary condition to stabilize non-triangular structures. Recently developed inverse statistical-mechanical methods have been indeed used to engineer purely repulsive and convex interaction potentials that yield complex ground-state crystals such as honeycomb lattice [28–32]. In the following, we want to develop a general method to predict the occurrence of complex non-triangular phases for a given pair interaction based on the enthalpy-like pair potential introduced in Sec. II C.

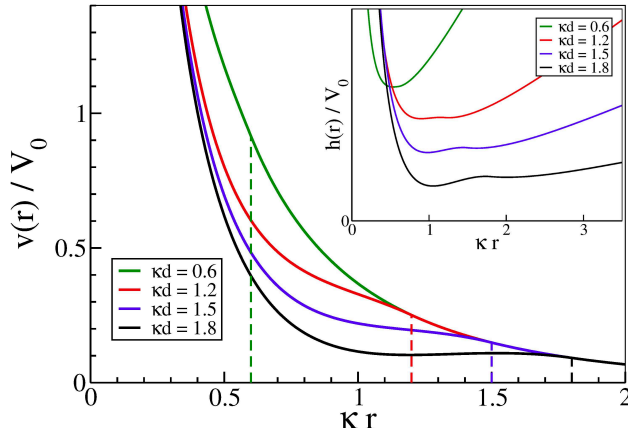


FIG. 2. Characteristic examples of pair interaction potentials  $v(r)$  as given by Eq. 1. Potentials are shown for three different reduced depletion lengths ( $\kappa d = 0.6, 1.2, 1.5, 1.8$ ), where the depletion lengths are indicated by the dashed lines. The inset illustrates the enthalpy-like pair interaction for  $\kappa d = 0.6, 1.2, 1.5, 1.8$  at  $\sqrt{\rho}d = 1.1$  as defined in Eq. 4. Although  $v$  for  $\kappa d = 1.2$  and  $\kappa d = 1.5$  does not possess any local maxima and minima, the corresponding  $h$  features a concave region separating two minima with a local maximum, yielding the stability of complex structures with multiple length scales, whereas  $h$  for  $\kappa d = 0.6$  lacks the existence of any concave region. Note that, in the inset, the enthalpy-like pair interactions are arbitrarily shifted along the  $y$ -axis for the sake of clarity.

In the following, we analyze the conditions under which  $h(r)$  might exhibit two minima. Note that, unlike the pair interaction potential  $v(r)$ , the explicit form of  $h(r)$  depends on the density via the macroscopic pressure  $p$ , cf. Eq. 4. The pressure  $p$  is given by  $p = -\partial U/\partial A$  where in the vicinity of a given particle  $i$  we can use  $dA_j = d(\pi r_{ij}^2) = 2\pi r_{ij} dr_{ij}$  as the change in the area and the energy per particle  $u = U/N = \sum_{i,j,i \neq j} v(r_{ij})/2N \approx \sum_j v(r_{ij})$  for  $T = 0$  such that  $p/N \approx -\sum_j \frac{1}{2\pi r_{ij}} \partial v(r_{ij})/\partial r_{ij}$  in the ground state. The prefactor  $C(\rho, Z, \tilde{\delta}) = 2\pi\tilde{\delta}a_1/\kappa Z = \sqrt{8\pi\tilde{\delta}}/(\sqrt{\sqrt{3}\kappa Z\sqrt{\rho}})$  is obtained from Eq. 6 which assumes areas of circular rings of a given thickness  $\tilde{\delta}$  and with radii given by distances that occur in a triangular lattice. At each density and depletion length, we calculate  $C(\rho, Z, \tilde{\delta})$  and  $p/N$  for our reference system, i.e., the triangular lattice, and determine  $h(r) = v(r) + 2\frac{p}{N}C(\rho, Z, \tilde{\delta})\kappa r$ .

In Fig. 1 we illustrate the phase space where  $h$  possesses two local minima with a concave region between them by the red area (using  $\tilde{\delta} \approx 0.4$ ). Within and only within the red area in Fig. 1, we expect the stability of complex non-triangular phases if stability is dominated by the closest neighbors. If, however, the closest-neighbor distance in a non-triangular crystal deviates only slightly from the triangular lattice constant at the same density, it is then upon further neighbors whether the triangular or the non-triangular one becomes stable.

For example, some regular phases like the square phase or rhombic phases that are morphologically close to the square phase are dominated by one nearest-neighbor length scale exactly as the triangular phase and therefore whether a triangular, a square or such a rhombic phase is stable not only depends on the closest neighbors. As a consequence, our theory can correctly predict a subdomain of the non-triangular stability region, and thus the red area shown in Fig. 1 differs from the non-triangular yellow area obtained by ground-state calculations, if, e.g., a square phase occurs.

Attention must be paid when interpreting the red stability region of non-triangular complex phases as predicted by our theory, see Fig. 1, where  $h(r)$  possesses a concave region separating two local minima. The triangular phase within this area only becomes unstable if one of the particles of the triangular structure is actually located in the concave region of  $h(r)$ . For large  $\kappa d$ , however, concave regions might occur in places where there is no particle in a triangular phase such that the triangular phase remains stable. As a consequence, the red area extends outside of the exact stability zone of the non-triangular phases obtained by ground-state calculations.

As opposed to the situation above, our theory captures very well the occurrence of some regular (e.g., elongated rhombic phases as shown in Fig. 5b) and complex phases (e.g., honeycomb, cluster phases, etc.) that are dominated by two nearest neighbors with distances sufficiently distinct from the triangular lattice constant. Recall that if nearest-neighbor distances are similar to the triangular length scale, the stability of the corresponding phase over the stability of the triangular phase is up to farther particles, and thus our approach may not necessarily yield a solid prediction of those phases. Consequently, the phases with two length scales fairly deviating from the triangular one can only occur within the red area. As an example; the hatched area in Fig. 1 indicates a subspace of non-triangular phases with stable regular and complex phases whose nearest-neighbor distances differ at least 15 per cent of the triangular lattice constant at the same density. Note that the choice of such a distance cutoff is rather not unique. However, we observe the same qualitative picture for different cutoffs above 10 percent.

To demonstrate the explicit form of the enthalpy-like pair potential  $h(r)$  in contrast to the pair potential  $v(r)$ , we plot  $h(r)$  in the inset of Fig. 2 for  $\kappa d = 0.6, 1.2, 1.5, 1.8$  with  $\tilde{p} \equiv 2pC/NV_0 \approx 2.63, 0.41, 0.20, 0.10$ , respectively. These reduced pressure values are obtained at  $\sqrt{\rho}d = 1.1$ . Three of them, namely  $\kappa d = 1.2, 1.5, 1.8$  show a clear local maximum alongside the two minima, whereas  $h$  for  $\kappa d = 0.6$  lacks completely such a situation for any density. A comparison with Fig. 1 confirms our conjecture that if  $h(r)$  has no concave region such as for  $\kappa d = 0.6$ , then we do not expect the stability of complex phases with multiple length scales that are fairly distinct from the triangular length scale.

Note that concerning the whole system, we are in an  $NVT$ -ensemble such that employing an enthalpy-like quantity is obviously unusual. This being said, we try to find a local criterion that can be used to predict the global structure from local properties. The local structure of an infinite thermodynamic system as given by a particle and its neighbors does not necessarily possess the same thermodynamic properties as the global structure. However, for a given reference structure, the local arrangement clearly depends on the pressure such that locally a free enthalpy-like quantity controls the order. Accordingly, at zero temperature an enthalpy-like function as we introduced here can be used to primarily predict the occurrence of structures with multiple length scales.

The global order is still reflected by the pressure as well as the functional form  $a(r)$  used in order to determine  $h(r)$ . As a consequence in principle  $h(r)$  has to be determined for different candidate structures, in order to check whether the corresponding candidate structure minimizes the total enthalpy  $H$  as given in Eq. 3. However, since the functional form in Eq. (7) is a good approximation to many lattices, the enthalpy-like function obtained by this choice for  $a(r)$  can be used to check whether the triangular order is stable or not. Furthermore, it is noteworthy that our criterion for non-triangular order does not take three-body or other multi-body interactions into account.

To summarize the results of this section, by determining the enthalpy-like pair potential  $h(r)$  for triangular lattices we can predict the parameters where triangular order or other symmetries dominated by only one length scale can become unstable, namely if  $h(r)$  possesses a concave part. Furthermore, we know that complex phases that are dominated by two distances between nearest neighbors can only occur if such a concave part exists. Note that instead of complex phase with two or more length scales in principle also a coexistence between phases with different length scales might occur. By refining our method by including not only the closer neighbor structure, it should be able to improve the predictions. However, then the determination of  $h(r)$  would become much more complicated and the benefit of a criterion that can be checked very easily for many parameters would be lost.

In Sec. IIIC we analyze in detail which phases can occur for the example of a colloid-polymer mixture if the triangular phase is not stable. In the next subsection, we first discuss the differences between the calculated ground-state results and our simulation results for finite temperature.

### B. Zero- vs. finite-temperature results

We have investigated the phase diagram of colloid-polymer mixtures at finite temperatures by means of Brownian dynamics computer simulations. Particularly, we consider a temperature such that  $V_0/k_B T =$

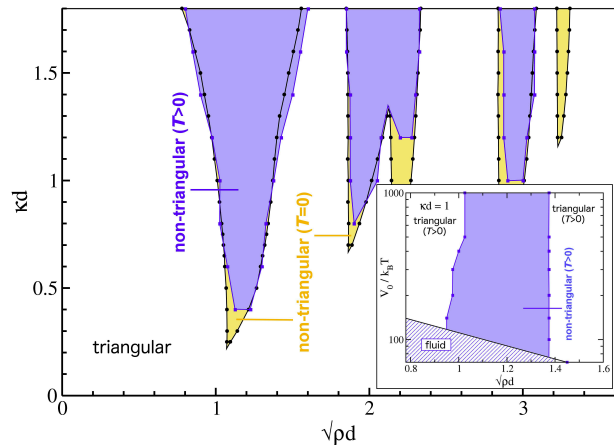


FIG. 3. Comparison of zero- and finite-temperature phase diagrams of colloid-polymer mixtures as a function of the reduced density  $\sqrt{\rho d}$  and the reduced depletion length  $\kappa d$ . The non-triangular stability modes as determined by lattice-sum minimizations and Brownian Dynamics simulations are shown by yellow (at  $T = 0$ ) and blue (at  $T > 0$ ) regions, respectively. The actual determined phase points at the boundary are indicated by black dots and blue squares. The inset shows the solid- and fluid-state phase diagram as a function of the reduced density and the reduced inverse temperature at fixed  $\kappa d = 1$ . Details are explained in the text.

1000 and we fix the energy amplitudes to  $V_0/W_0 = 1$ . We reveal the stability of non-triangular crystals in the blue regions shown in Fig. 3. The similarity to the non-triangular stability regimes at  $T = 0$  (shown in yellow in Fig. 3) is striking. Specifically, in both cases, the majority of the parameter space in the  $(\sqrt{\rho d}, \kappa d)$ -plane is governed by the triangular crystal as shown by the white region in Fig. 3. Non-triangular phases only occur in the vicinity of specific densities and for sufficiently large values of  $\kappa d$ .

Moreover, the inset of Fig. 3 provides the evolution of the non-triangular solid phase space at  $\kappa d = 1$  as a function of the inverse reduced temperature where melting is observed upon rising the temperature. Note also that at finite temperatures, the system melts as  $\sqrt{\rho d} \rightarrow 0$ . The melting is, however, out of the scope of this paper, and therefore not analyzed further here.

Another striking feature in simulations is that we observe phases of almost all of the different phase categories as enlisted and explained in the next subsection. As the main goal of this manuscript is to provide a postulate based on which complex crystals can be predicted and compare the theoretical predictions to numerical results at  $T = 0$ , simulations are just supposed to serve as additional data to strengthen the ground-state results. Therefore, we choose to show only a few characteristic simulation snapshots rather than describing the finite-temperature phase diagram thoroughly.



### C. Detailed phase diagram of a colloid-polymer mixture

In the following, we explore the ground-state phase diagram of a colloid-polymer mixture in detail. The stability of zero-temperature crystalline phases are shown in Fig. 4 for  $\sqrt{\rho d} \leq 2.5$  and  $\kappa d \leq 1.8$ . In Fig. 4 we show

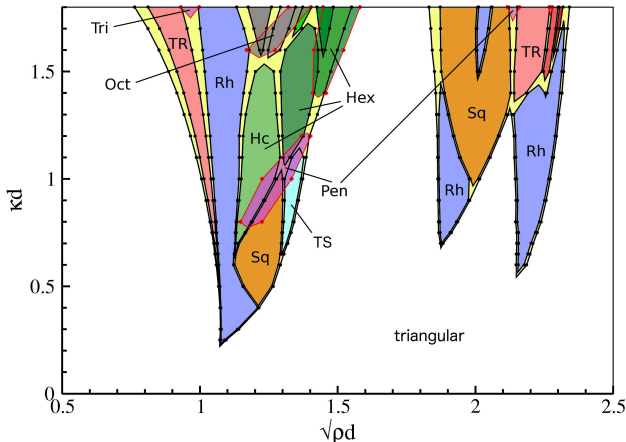


FIG. 4. Detailed zero-temperature phase diagram of a colloid-polymer mixture as a function of the reduced density  $\sqrt{\rho d}$  and the reduced depletion length  $\kappa d$ . The large white zone indicates the stability of the triangular phase, whereas other colors have been used to demonstrate the non-triangular stability regimes that include a variety of phase structures, each colored differently and labeled as follows: Sq: square phase, Rh: rhombic phase, Hex: hexagon-based structures including the honeycomb (Hc) lattice, Oct: octagon-based structures, Tri: trimers, TR: triangle-rectangular structures, TS: triangle-square structures, and Pen: pentagon-based structures. The black dots are the actual computed phase points at the boundary of non-triangular phases. The yellow areas illustrate the coexistence between the neighboring phases. The phases are shown for up to 4 particles per unit cell. The regions where we find additional phases with 5 or 6 particles per unit cell are marked by transparent colors. While outside of these regions we do not expect the occurrence of phases with even more particles per unit cell, within the transparent regions more complex phases might be stable.

the detailed phase behavior for the first non-triangular regions with lowest density. The phase diagram reveals a large structural diversity. The white region indicates the stability regime of the triangular lattice as before, whereas the colored areas demonstrate the occurrence of stable non-triangular phases of different symmetry and complexity. Here, we obtain simple phases with  $n = 1$  particle per unit cell such as rhombic (Rh) and square (Sq) lattices as shown by blue and orange regions in Fig. 4 as well as more complex structures with  $n \geq 2$ . The latter possess a richer diversity and can be grouped into hexagon-based (Hex, green regions) structures including the honeycomb (Hc) lattice, octagon-based (Oct, gray regions) structures, trimers (Tri, purple), triangle-rectangular (TR, red regions), and triangle-square (TS,

turquoise region) structures, and finally the pentagon-based (Pen, purple transparent regions) structures as indicated by different colors and labeled accordingly in Fig. 4. Structural details are provided below.

For the sake of completeness, we further investigated the phase coexistence in our system: We have implemented the common tangent construction (Maxwell construction) and have determined the corresponding coexistence regimes between two neighboring phases, which we indicate by the yellow areas in the phase diagram in Fig. 4. As expected, the coexistence turns out to be relatively small at zero-temperature as compared to pure one-phase stability regimes.

The phases in Fig. 4 are shown for up to 4 particles per unit cell with solid colors. In addition, the regions where 5 or 6 particles per unit cell lead to new phases are marked by transparent colors encircled by the red lines. While outside of these regions we do not have any indication for the occurrence of phases with even more particles per unit cell, within the transparent regions more complex phases might be expected to be stable.

#### 1. Triangular (Tr), rhombic (Rh), and square (Sq) phases

The ground-state phase diagram exhibits three simple crystalline phases, namely the triangular, rhombic, and square phases that are each shown in the left panels of Figs. 5a, b, and c, respectively. The red lines serve as a guide to the eye showing the trivial unit cells in each structure. Characteristic snapshots of simple phases from finite-temperature BD simulations at  $V_0/k_B T = 1000$  are displayed in the right panels of Figs. 5a, b, and c.

We further identify plenty of complex structures containing at least two particles per unit cell. To achieve a clear overview for the reader, we choose to present them in groups according to the main repeating structural unit of each phase. Each group is uniquely color-coded in Fig. 4 as we use different colors and its shades for different groups. In the following, we list these groups alongside with structural images, and for clarity, we further regard the resulting structures as tilings, and we illustrate their prototiles.

#### 2. Hexagon-based structures (Hex)

Hexagon-based structures appear in the first non-triangular region, albeit comprising regular hexagons as their main periodically repeating unit. For the sake of clarity, we provide a further point of view on the structures in the remainder of this paper: In addition to the unit cells that are marked red, we show the characteristic prototiles of the corresponding tilings by green lines in each figure. In this case, the prototiles are either a hexagon or a hexagon together with one or two distinct triangles as indicated by the green lines in Fig. 6. One

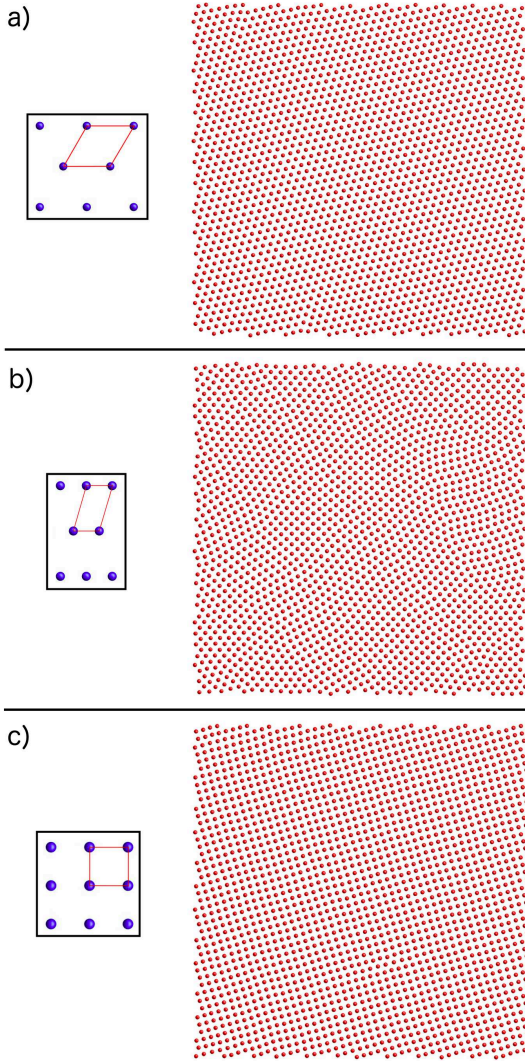


FIG. 5. Triangular (a), rhombic (b), and square (c) phases at  $T = 0$  (left panels) as obtained by lattice-sum minimizations and  $T > 0$  (right panels) as obtained by Brownian Dynamics simulations. The red lines on the left panels depict the unit cells of the structures. The simulations contain  $N = 2000$  particles.

of these structures corresponds to the well-known honeycomb lattice (upper left in Fig. 6), whereas the other four consist of hexagons and triangles each in different stoichiometric ratios. This group is indicated by shades of green in Fig. 4 including the green transparent region with  $n = 5, 6$ . The latter are shown in the lower panel of Fig. 6.

The honeycomb lattice coincides with one of the three Platonic (regular) tilings, namely the hexagonal tiling, whereas the other two Platonic tilings are the trivial triangular and square ones which are obtained from the triangular and square lattice by connecting the nearest neighbors to each other to constitute the prototiles. The structure on the right hand side in the lower panel of Fig. 6 corresponds to one of the eight Archimedean tilings, namely to the so called *snub trihexagonal tiling*.

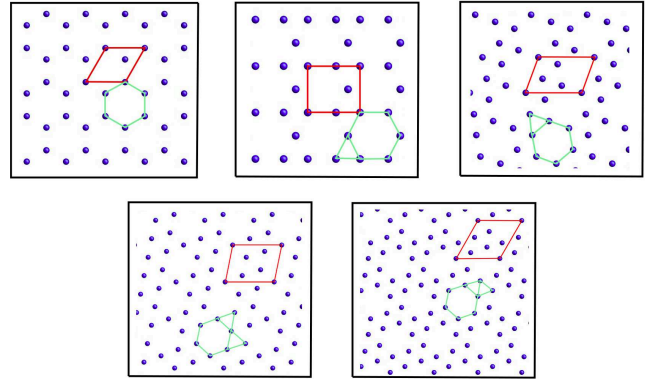


FIG. 6. Schematic illustration of five stable hexagon-based structures with regular hexagons as their main repeating units at  $T = 0$  as obtained by lattice-sum minimizations. Different prototiles of the corresponding tilings are indicated by green lines. These are either one hexagon or an hexagon with one or two different triangles. Note that the upper left structure corresponds to the honeycomb lattice. Red lines emphasize the unit cells with  $n = 2, \dots, 6$ .

### 3. Octagon-based structures (Oct)

Octagon-based structures occur in the first non-triangular stability mode for  $\kappa d > 1.5$  and  $1.2 < \sqrt{\rho}d < 1.4$  and they are colored gray in Fig. 4 including the gray transparent region. We identify five different structures with a non-regular octagon as the main repeating unit, where four of them tile the space together with one or two different triangles (not necessarily equilateral). Hence, the prototiles are an octagon and one or two triangles as indicated by green lines in Fig. 7. The red lines show a minimal unit cell for each structure.

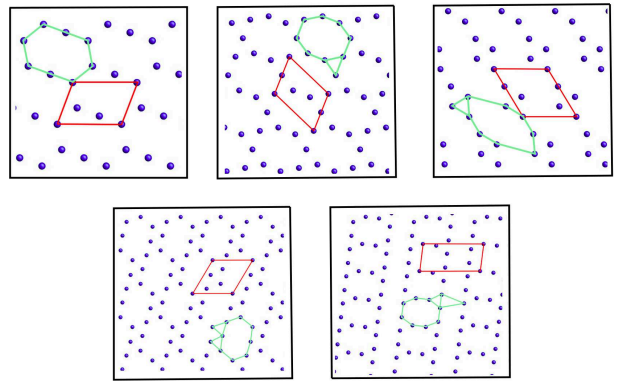


FIG. 7. Schematic illustration of five stable octagon-based structures with non-regular octagons as their main repeating units at  $T = 0$  as obtained by lattice-sum minimizations. The prototiles of the corresponding tilings are either one octagon or an octagon with one or two different triangles as indicated by green lines. Red lines mark the unit cells with  $n = 3, 4, 5$ .



#### 4. Trimers (Tri)

The trimer phase is found at  $\kappa d > 1.7$  and  $\sqrt{\rho}d \approx 0.9$  with the corresponding phase structures involving two well-separated length scales per dimension. The larger one dictates the periodicity of the overall lattice, whereas at the smaller length scale, the particles are arranged in equilateral triangles as a basis, see Fig. 8. The corresponding tiling possesses four distinct triangles as indicated by the green lines in the same figure, where also a unit cell with  $n = 6$  is demonstrated by red lines.

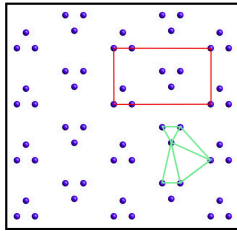


FIG. 8. Schematic illustration of a stable trimer structure at  $T = 0$  as obtained by lattice-sum minimizations. The corresponding tiling can be constructed by four different triangles as its prototiles which are shown by green lines. Red lines mark the unit cell with  $n = 6$ .

#### 5. Triangle-rectangular structures (TR)

Here, we reveal four different types of lattice structures, where we choose to demonstrate the lattice points as arranged in triangles and rectangles as basic constituents (prototiles of the corresponding tilings, cf. green lines in Fig. 9). Each structure possesses a different ratio between these constituents. The upper left structure of Fig. 9 occurs in the first non-triangular stability mode ( $\sqrt{\rho}d < 1.1$ ), whereas the others are identified for  $\kappa d > 1.3$  and  $2.1 < \sqrt{\rho}d < 2.3$ . The stability zones are shown by red areas in Fig. 4. As usual, the red lines in Fig. 9 depict the unit cells with  $n = 2, \dots, 5$ .

#### 6. Triangle-square structures (TS)

Triangle-square phase is indicated by the turquoise region in the phase diagram in Fig. 4 with the phase structure possessing four particles in the unit cell (cf. red lines in Fig. 10). The corresponding tiling consisting of equilateral triangles and squares as specified by the green lines in Fig. 10 is revealed to be the *snub square* tiling, also known as  $\sigma$ - or H-phase, which corresponds to one of the eight Archimedean tilings.

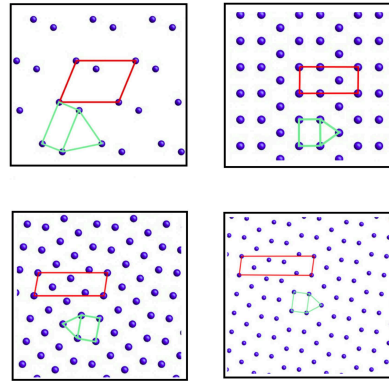


FIG. 9. Schematic illustration of four stable triangle-rectangular structures at  $T = 0$  as obtained by lattice-sum minimizations. The corresponding tiling has a rectangle and a triangle as its prototiles, whereas the ratio between them differs in each structure. Red lines mark the unit cells with  $n = 2, \dots, 5$ .

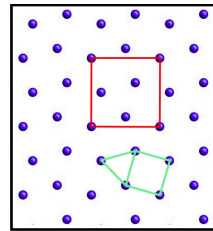


FIG. 10. Schematic illustration of a stable triangle-square structure at  $T = 0$  as obtained by lattice-sum minimizations. It composes of a square and a triangle as the prototiles of the corresponding tiling. Red lines mark the unit cell with  $n = 4$ .

#### 7. Pentagon-based structures (Pen)

In this group, we have four perfect ground-state lattice structures possessing  $n = 5$  ( $n = 6$ ) as shown in the upper (lower) level of Fig. 11a, with the red lines indicating the corresponding unit cells. These structures are found in a relatively broad regime in the first non-triangular stability mode for  $1.1 < \sqrt{\rho}d < 1.4$  around  $\kappa \approx 1$  as well as in a tiny regime for  $\sqrt{\rho}d \approx 2.15$  and  $\kappa d > 1.7$ . These regions are indicated by the purple transparent areas in Fig. 4.

As seen in Fig. 11a, the pentagon-based structures differ in the type and number of prototiles, that is, some of them tile the space periodically by just one non-regular pentagon, whereas others need (beside the pentagon) one or two different triangles or a triangle and a square.

In Fig. 11b, we demonstrate two characteristic snapshots of finite-temperature simulations showing clear local pentagonal orderings. Black dots represent particle positions, whereas red lines have been introduced to connect the nearest neighbors based on a distance criterion, and thus to highlight a possible tessellation of the space with pentagons. The basic difference between

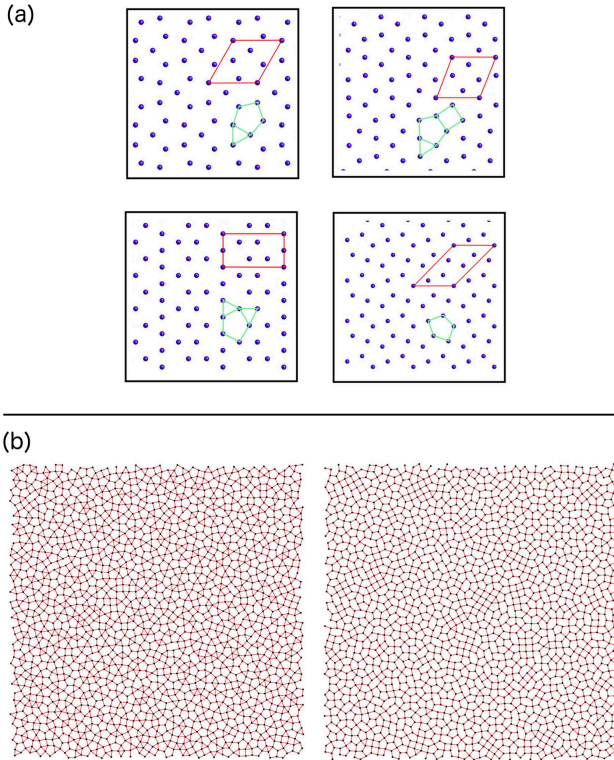


FIG. 11. Stable pentagon-based structures at (a)  $T = 0$  as obtained by lattice-sum minimizations and (b)  $T > 0$  with non-regular pentagons being the main repeating unit as obtained by Brownian Dynamics simulations. The four crystalline ground-state structures are schematically illustrated in (a), where green lines indicate the different prototypes of the corresponding tilings, and red lines emphasize the unit cell in each structure. In (b), two characteristic simulation snapshots are shown exhibiting high local pentagonal order and resembling some of the pentagon-based structures from (a).

both snapshots in Fig. 11b is that the left one comprises predominantly pentagons and rhombuses as tiles, whereas in the right image there exists a considerable amount of triangles beside the pentagons, suggesting a strong resemblance to the ground-state structure shown on the upper left in Fig. 11a. We would like to mention that we have undertaken different runs starting from random, triangular, and square lattice configurations, and all runs lead to very similar final configurations displaying the same local pentagonal orderings at prescribed system parameters.

Our lattice-minimization routine reveals solely the stability of perfect lattices at zero-temperature. Having the possibility of stable non-periodic structures in mind, we have included some quasicrystalline orderings according to the Penrose-, square-triangle- and square-rhombic-tiling into our calculations by computing the potential energies per particle of large periodic approximants of the corresponding quasiperiodic tilings. As a result, within the studied parameter range, we have not observed any stable quasicrystalline phase.

#### IV. CONCLUSIONS

In summary, we have developed a theoretical tool to predict the self-assembly of complex phase structures in classical condensed matter systems where thermodynamic stability is dictated by pair interactions. Our theory involves the enthalpy-like pair potential. We conjecture that complex non-trivial orderings can occur if the enthalpy-like potential rather than the pair interaction itself possesses a concave region. In order to validate our theory, we studied the specific example of two-dimensional colloid-polymer mixtures, which we have modeled with effective pair interactions involving a short-ranged depletion attraction and a long-ranged screened electrostatic Coulomb repulsion. In particular, we have investigated a detailed zero-temperature phase diagram of our system and we have analyzed the validity of occurring phases at finite but relatively small temperatures  $T > 0$ . We found a remarkable agreement between our theory and ground-state calculations as we revealed that our theory can identify relatively good the parameter region where complex structures with two or more length scales are stable.

Furthermore, our ground-state phase diagram exhibits a rich morphology: First of all, we identify large regions of triangular-lattice stability, and regions of non-triangular lattices appearing as stability modes as a function of the density at fixed depletion length and polymer concentration. Second of all, the non-triangular regimes themselves feature a large diversity with respect to the stable phases. We recover simple phases such as rhombic and square lattices, but more interestingly, we also reveal complex phase structures with pentagon-, hexagon-, and octagon-based structures as well as trimers, triangle-rectangular and triangle-square crystals, some of which are also found to be stable at  $T > 0$ , and some others not. Furthermore, some of these ground-state structures correspond to the well-known Archimedean tilings, self-assembly of which has attracted a special interest in fundamental and applied physical sciences [63–65].

Ground state calculations can always depend on the candidate structures that are considered. We have determined all phases that are obtained for up to  $n = 6$  particles per unit cell, where we show the phases for up to  $n = 4$  particles per unit cell and indicate how an inclusion of  $n = 5, 6$  particles into our minimization process yields slight changes shown by the transparent regions encircled by the red lines. The overall change when increasing the number of particles per unit cell is marginal and hence we only expect non-significant morphology changes of the non-triangular stability regions in the phase diagram in Fig. 4 upon an inclusion of  $n > 6$  particles per unit cell. Our Brownian Dynamics simulations confirm the triangular, square, rhombic, and pentagon-based structures. However, it is noteworthy that occurrence of exotic phases other than hitherto found ones within the stability zone of non-triangular

lattices cannot be ultimately excluded.

Our investigations have fundamental implications as we identified the ground-state phase diagram of colloid-polymer mixtures alongside a zoo of novel structures occurring in the same system, and practical implications as we establish systematic routes for the self-assembly of complex structures. These phases should be accessible in experiments and therefore our phase diagram explains how to tailor complex colloidal structures that might, e.g., be of interest for photonic applications.

Finally, we want to stress that our theory involving the enthalpy-like pair potential can be applied to all particle interactions according to isotropic pair poten-

tials and that it opens far-reaching possibilities to explore the self-assembly in numerous condensed matter phases.

## ACKNOWLEDGMENTS

We would like to thank A. S. Kraemer, F. Martelli, and R. E. Rozas for illuminating discussions. E.C.O. and M.S. received financial support from the SFF of the HHU Düsseldorf. Furthermore, A.M. and M.S. were supported by the DFG within the Emmy Noether program (Grant Schm2657/2).

- 
- [1] G. M. Whitesides, J. P. Mathias, and C. T. Seto. Molecular self-assembly and nanochemistry: a chemical strategy for the synthesis of nanostructures. *Science*, 254:1312–1319, 1991.
  - [2] G. M. Whitesides and B. Grzybowski. Self-assembly at all scales. *Science*, 295:2418, 2002.
  - [3] G. M. Whitesides and M. Boncheva. Beyond molecules: Self-assembly of mesoscopic and macroscopic components. *Proc. Nat. Acad. Sci.*, 99:4769–4774, 2002.
  - [4] R. Groß and M. Dorigo. Self-assembly at the macroscopic scale. *Proc. IEEE*, 96:1490–1508, 2008.
  - [5] J.-M. Lehn. Toward self-organization and complex matter. *Science*, 295:2400–2403, 2002.
  - [6] S. A. Jenekhe and X. L. Chen. Self-assembly of ordered microporous materials from rod-coil block copolymers. *Science*, 283:372, 1999.
  - [7] A. M. Jackson, J. W. Myerson, and F. Stellacci. Spontaneous assembly of subnanometre-ordered domains in the ligand shell of monolayer-protected nanoparticles. *Nat. Mater.*, 3:330, 2004.
  - [8] V. N. Manoharan, M. T. Elsesser, and D. J. Pine. Dense packing and symmetry in small clusters of microspheres. *Science*, 301:483, 2003.
  - [9] W. M. Jacobs and D. Frenkel. Self-assembly of structures with addressable complexity. *J. Am. Chem. Soc.*, 138:2457–2467, 2016.
  - [10] D. J. Kushner. Self-assembly of biological structures. *Bacteriol Rev.*, 33:302–345, 1969.
  - [11] Y. Engelborghs. Microtubules: dissipative structures formed by self-assembly. *Biosensors & Bioelectronics*, 9:685–689, 1994.
  - [12] E. O. Budrene and H. C. Berg. Dynamics of formation of symmetrical patterns by chemotactic bacteria. *Nature*, 376:49–53, 1995.
  - [13] J. D. Halley and D. A. Winkler. Critical-like self-organization and natural selection: Two facets of a single evolutionary process? *BioSystems*, 92:148–158, 2008.
  - [14] T. Dotera, T. Oshiro, and P. Ziherl. Mosaic two-lengthscale quasicrystals. *Nature*, 506:208–211, 2014.
  - [15] D. Shechtman, I. Blech, D. Gratias, and J. W. Cahn. Metallic phase with long range orientational order and no translation symmetry. *Phys. Rev. Lett.*, 53:1951–1954, 1984.
  - [16] L. Assoud, R. Messina, and H. Löwen. Stable crystalline lattices in two-dimensional binary mixtures. *Eur. Phys. Lett.*, 80:48001, 2007.
  - [17] L. Assoud, R. Messina, and H. Löwen. Binary crystals in two-dimensional two-component yukawa mixtures. *J. Chem. Phys.*, 129:164511, 2008.
  - [18] M. Antlanger and G. Kahl. Wigner crystals for a planar, equimolar binary mixture of classical, charged particles. *Condens. Matter Phys.*, 16:43501, 2013.
  - [19] P. F. Damasceno, M. Engel, and S. C. Glotzer. Predictive self-assembly of polyhedra into complex structures. *Science*, 337:453–457, 2012.
  - [20] Q. Chen, S. C. Bae, and S. Granick. Directed self-assembly of a colloidal kagome lattice. *Nature*, 469:381, 2011.
  - [21] G. Doppelbauer, E. G. Noya, E. Bianchi, and G. Kahl. Self-assembly scenarios of patchy colloidal particles. *Soft Matter*, 8:7768, 2012.
  - [22] E. Bianchi, C. N. Likos, and G. Kahl. Tunable assembly of heterogeneously charged colloids. *Nano Lett.*, 14:3412–3418, 2014.
  - [23] M. Rechtsman, F. H. Stillinger, and S. Torquato. Optimized interactions for targeted self-assembly: Application to a honeycomb lattice. *Phys. Rev. Lett.*, 95:228301, 2005.
  - [24] M. Rechtsman, F. H. Stillinger, and S. Torquato. Designed interaction potentials via inverse methods for self-assembly. *Phys. Rev. E*, 73:011406, 2006.
  - [25] R. D. Batten, F. H. Stillinger, and S. Torquato. Classical disordered ground states: Super-ideal gases and stealth and equi-luminous materials. *J. Appl. Phys.*, 104:033504, 2008.
  - [26] S. Torquato. Inverse optimization techniques for targeted self-assembly. *Soft Matter*, 5:1157–1173, 2009.
  - [27] H. Cohn and A. Kumar. Algorithmic design of self-assembling structures. *Proc. Nat. Acad. Sci.*, 106:9570–9575, 2009.
  - [28] É. Marcotte, F. H. Stillinger, and S. Torquato. Unusual ground states via monotonic convex pair potentials. *J. Chem. Phys.*, 134:164105, 2011.
  - [29] A. Jain, J. R. Errington, and T. M. Truskett. Inverse design of simple pairwise interactions with low coordinated 3d lattice ground states. *Soft Matter*, 9:3866, 2013.
  - [30] A. Jain, J. R. Errington, and T. M. Truskett. Dimensionality and design of isotropic interactions that stabilize honeycomb, square, simple cubic, and diamond lattices. *Phys. Rev. X*, 4:031049, 2014.

- [31] W. D. Piñeros, M. Baldea, and T. M. Truskett. Designing convex repulsive pair potentials that favor assembly of kagome and snub square lattices. *J. Chem. Phys.*, 145:054901, 2016.
- [32] W. D. Piñeros, M. Baldea, and T. M. Truskett. Breadth versus depth: Interactions that stabilize particle assemblies to changes in density or temperature. *J. Chem. Phys.*, 144:084502, 2016.
- [33] R. Castañeda-Priego, A. Rodríguez-López, and J. M. Méndez-Alcaraz. Depletion forces in two-dimensional colloidal mixtures. *J. Phys.: Condens. Matter*, 15:S3393–S3409, 2003.
- [34] P. Domínguez-García. Microrheological consequences of attractive colloid-colloid potentials in a two-dimensional brownian fluid. *Eur. Phys. J. E*, 35:73, 2012.
- [35] L. Feng, B. Laderman, S. Sacanna, and P. Chaikin. Re-entrant solidification in polymer-colloid mixtures as a consequence of competing entropic and enthalpic attractions. *Nat. Mater.*, 14:61–65, 2015.
- [36] K. N. Pham, A. M. Puertas, J. Bergenholtz, S. U. Egelhaaf, A. Moussaid, P. N. Pusey, A. B. Schofield, M. E. Cates, M. Fuchs, and W. C. K. Poon. Multiple glassy states in a simple model system. *Science*, 296:104–106, 2002.
- [37] T. Eckert and E. Bartsch. Re-entrant glass transition in a colloid-polymer mixture with depletion attractions. *Phys. Rev. Lett.*, 89:125701, 2002.
- [38] S. Manley, H. M. Wyss, K. Miyazaki, J. C. Conrad, V. Trappe, L. J. Kaufman, D. R. Reichman, and D. A. Weitz. Glasslike arrest in spinodal decomposition as a route to colloidal gelation. *Phys. Rev. Lett.*, 95:238302, 2005.
- [39] P. J. Lu, E. Zaccarelli, F. Ciulla, A. B. Schofield, F. Sciortino, and D. A. Weitz. Gelation of particles with short-range attraction. *Nature*, 453:499–504, 2008.
- [40] I. Zhang, C. P. Royall, M. A. Faers, and P. Bartlett. Phase separation dynamics in colloid-polymer mixtures: the effect of interaction range. *Soft Matter*, 9:2076–2084, 2013.
- [41] Ethayaraja Mani, Wolfgang Lechner, Willem K. Kegels, and Peter G. Bolhuis. Equilibrium and non-equilibrium cluster phases in colloids with competing interactions. *Soft Matter*, 10:4479–4486, 2014.
- [42] M. Kohl, R. F. Capellmann, M. Laurati, S. U. Egelhaaf, and M. Schmiedeberg. Directed percolation identified as equilibrium pre-transition towards non-equilibrium arrested gel states. *Nat. Commun.*, 7:11817, 2016.
- [43] A. Stradner, H. Sedgwick, F. Cardinaux, W. C. K. Poon, S. U. Egelhaaf, and P. Schurtenberger. Equilibrium cluster formation in concentrated protein solutions and colloids. *Nature*, 432:492–495, 2004.
- [44] J. Taffs, A. Malins, S. R. Williams, and C. P. Royall. A structural comparison of models of colloid-polymer mixtures. *J. Phys.: Condens. Matter*, 22:104119, 2010.
- [45] F. Leal Calderon, J. Bibette, and J. Biais. Experimental phase diagrams of polymer and colloid mixtures. *EPL (Europhysics Letters)*, 23(9):653, 1993.
- [46] M. Dijkstra, R. van Roij, and R. Evans. Phase diagram of highly asymmetric binary hard-sphere mixtures. *Phys. Rev. E*, 59:5744–5771, 1999.
- [47] M. Schmidt, H. Löwen, J. M. Brader, and R. Evans. Density functional theory for a model colloid-polymer mixture: bulk fluid phases. *J. Phys.: Condens. Matter*, 14:9353–9382, 2002.
- [48] W. C. K. Poon. The physics of a model colloid-polymer mixture. *J. Phys.: Condens. Matter*, 14:R859–R880, 2002.
- [49] D. G. A. L. Aarts, R. Tuinier, and H. N. W. Lekkerkerker. Phase behaviour of mixtures of colloidal spheres and excluded-volume polymer chains. *Journal of Physics: Condensed Matter*, 14(33):7551, 2002.
- [50] C. P. Royall, D. G. A. L. Aarts, and H. Tanaka. Fluid structure in colloid-polymer mixtures: the competition between electrostatics and depletion. *J. Phys.: Condens. Matter*, 17:S3401–S3408, 2005.
- [51] A. Fortini, M. Dijkstra, and R. Tuinier. Phase behaviour of charged colloidal sphere dispersions with added polymer chains. *J. Phys.: Condens. Matter*, 17:7783–7803, 2005.
- [52] Gerard J. Fleer and Remco Tuinier. Analytical phase diagram for colloid-polymer mixtures. *Phys. Rev. E*, 76:041802, Oct 2007.
- [53] Gerard J. Fleer and Remco Tuinier. Analytical phase diagrams for colloids and non-adsorbing polymer. *Advances in Colloid and Interface Science*, 143(12):1–47, 2008.
- [54] R. Tuinier, P. A. Smith, W. C. K. Poon, S. U. Egelhaaf, D. G. A. L. Aarts, H. N. W. Lekkerkerker, and G. J. Fleer. Phase diagram for a mixture of colloids and polymers with equal size. *EPL (Europhysics Letters)*, 82(6):68002, 2008.
- [55] Álvaro González García and Remco Tuinier. Tuning the phase diagram of colloid-polymer mixtures via yukawa interactions. *Phys. Rev. E*, 94:062607, Dec 2016.
- [56] A. Moncho-Jordá, A. A. Loius, P. G. Bolhuis, and R. Roth. The asakura-oosawa model in the protein limit: the role of many-body interactions. *J. Phys.: Condens. Matter*, 15:S3429–S3442, 2003.
- [57] M. Dijkstra, R. van Roij, R. Roth, and A. Fortini. Effect of many-body interactions on the bulk and interfacial phase behavior of a model colloid-polymer mixture. *Phys. Rev. E*, 73:041404, 2006.
- [58] B. Cui, B. Lin, D. Frydel, and S. A. Rice. Anomalous behavior of the depletion potential in quasi-two-dimensional binary mixtures. *Phys. Rev. E*, 72:021402, 2005.
- [59] D. Frydel and S. A. Rice. Depletion interaction in a quasi-two-dimensional colloid assembly. *Phys. Rev. E*, 71:041402, 2005.
- [60] A. Fortini, M. Schmidt, and M. Dijkstra. Phase behavior and structure of model colloid-polymer mixtures confined between two parallel planar walls. *Phys. Rev. E*, 73:051502, 2006.
- [61] R. L. C. Vink, K. Binder, and J. Horbach. Critical behavior of a colloid-polymer mixture confined between walls. *Phys. Rev. E*, 73:056118, 2006.
- [62] J. Kepler. *Harmonices Mundi*. 1619.
- [63] M. Schmiedeberg, J. Mikhael, S. Rausch, J. Roth, L. Helden, C. Bechinger, and H. Stark. Archimedean-like colloidal tilings on substrates with decagonal and tetradecagonal symmetry. *Eur. Phys. J. E*, 32:25–34, 2010.
- [64] M. Antlanger, G. Doppelbauer, and G. Kahl. On the stability of archimedean tilings formed by patchy particles. *J. Phys.: Condens. Matter*, 23:404206, 2011.
- [65] J. A. Millan, D. Ortiz, G. van Anders, and S. C. Glotzer. Self-assembly of archimedean tilings with enthalpically



- and entropically patchy polygons. *ACS Nano*, 8:2918–2928, 2014.
- [66] S. Asakura and F. Oosawa. *J. Chem. Phys.*, 22:1255, 1954.
- [67] A. Vrij. *Pure Appl. Chem.*, 48:471, 1976.
- [68] J. A. Nelder and R. A. Mead. A simplex method for function minimization. *Computer Journal*, 7:308–313, 1965.
- [69] N. J. A. Sloane. Theta series and magic numbers for diamond and certain ionic crystal structures. *J. Math. Phys.*, 28:1653, 1987.
- [70] J. H. Conway and N. J. A. Sloane. *Sphere Packings, Lattices and Groups*. Springer, New York, 3rd edn. edition, 1999.
- [71] J. de Graaf, L. Filion, M. Marechal, R. van Roij, and M. Dijkstra. Crystal-structure prediction via the floppy-box monte carlo algorithm: Method and application to hard (non)convex particles. *J. Chem. Phys.*, 137:214101, 2012.